

A Surge Preceding Prominence Eruption on 2014 March 14: Case Study

Peter Duchlev¹, Momchil Dechev¹, Kostadinka Koleva²

¹ Institute of Astronomy and NAO, Bulgarian Academy of Sciences, BG-1784, Sofia,

² Space Research Institute, Bulgarian Academy of Sciences, BG-1000, Sofia
duchlev@astro.bas.bg

(Submitted on 06.03.2020; Accepted on 04.11.2020)

Abstract. We study the precursor phase, activation, and ejection of solar surge occurring on 2014 March 14. The surge was associated with an eruptive prominence (EP), several flares and partial-halo coronal mass ejection (CME). For our study we used EUV data from the Atmospheric Imaging Assembly on board of the Solar Dynamics Observatory. The surge occurred in a young active region in a flux emergence phase located beneath a multiple-arcade helmet streamer. The surge appeared at the footpoints of the EP massive flux rope (MFR) as a flare-like loop. The surge upward motion clearly showed two subphases: acceleration and deceleration ones. During the first subphase, the surge rose up to height of 45 Mm with growing speed in the range 3-65 km/s and accelerations from 0.5 m/s² to 129 m/s². During the second subphase, the surge began to rise with constant deceleration of -54.8 m/s² and a decreasing speed from 60 to 3 km/s. During the surge downward motion the plasma fell back with a speed of 27 km/s. The surge ejection revealed four episodes in its EUV brightening evolution. During the surge downflow phase, the EUV brightening enhancement at the footpoints of surge-EP system suggests surge mass impact at this place, which plays a key role in bright flux rope (BFR) initiation and formation underneath the slowly rising EP MFR. Taking into account the crucial role of the BFR for further EP evolution, we conclude that the EP was triggered by the surge via tether-cutting reconnection.

Key words: Sun, Surges, Prominence/Filament eruptions, Flares, EUV radiation, Multi-wavelength observations

Introduction

The solar surges are straight or slightly curved collimated ejections of dense plasma from the chromosphere into the coronal heights, which usually show a strong tendency for recurrence (Bruzek & Durrant, 1977; Li et al., 1996). Since, surges exhibit episodic heating and cooling, they may be observed in the range of emissions from H_{α} to UltraViolet (UV), Extreme UltraViolet (EUV) and X-rays, and can be abbreviated in general as solar jets (see Schmieder et al., 1995; Pariat et al., 2010, for detailed reviews). The surges may have an initiation velocity of ~ 50 km/s, which may further increase up to a maximum value of 100–300 km/s (Schmieder et al. 1994), and may reach up to heights of 10-200 Mm or even more (Sterling, 2000). The lifetime of surges may extent 30 minutes (Schmieder et al., 1994) or even 45 minutes (Bong et al., 2014), and they can be recurrent with a period of an hour or more (Schmieder et al., 1984, 1995). In addition, a part of the recurrent surges/jets exhibit a homologous behavior (Pariat et al., 2010). It has been reported that surges rise upwards then diffuse, fade out, and often returns into the chromosphere along the ascent trajectory (e.g. Bong et al., 2014). The rise and fall phases of surges are often observed accompanied by rotation or helical motions (e.g. Gu et al., 1994; Canfield et al., 1996; Bong et al., 2014, for reviews). In some cases of H_{α} surges (Canfield et al., 1996) and UV jets (Liu et al., 2011) the unwinding of

helical structures were reported. The authors argued that the twist of emerging flux is transferred to the reconnected fields via the interchange reconnection.

Observationally, surges often occur near sunspots (Rust, 1968; Kurokawa & Kawai, 1993), in the proximity of neutral line of the magnetic fields (Rust, 1968; Beck et al., 2007; Engell et al., 2011). They are associated with magnetic flux emergence and cancellation regions (Kurokawa&Kawai, 1993; Gaizauskas, 1996; Liu & Kurokawa, 2004) or converging magnetic systems (Schmieder et al., 1993; Canfield et al., 1996; Liu & Zhang, 2001). Previous observations support the idea that magnetic reconnection between emerging flux and overlying magnetic field plays a key role in the surge propagation (Shibata et al., 1992; Canfield et al., 1996; Shimojo et al., 1998; Chae et al., 1999). Besides, solar surges can also be triggered by the impulsive generation of a pressure pulse (Shibata et al., 1982; Sterling et al., 1993), or by reconnection-generated explosive events (Madjarska et al., 2009).

Previous observational studies have found a close relationship between surge/jet activity and the basic solar eruptive events, i.e. flares, eruptive prominences/filaments and CMEs. The emergence and evolution of solar surges are often associated with flares (e.g. Schmieder et al., 1988, 1995; Uddin et al., 2004, 2010; Chandra et al., 2006; Joshi et al., 2016; Panesar et al., 2016). In multi-wavelength observational study, Uddin et al. (2012) reported for energy buildup and dynamics in the form of multiple surge eruptions associated with flares, due to successive reconnections initiated by magnetic flux cancellations.

Occasionally, jets are associated with large-scale solar eruptions, such as filament eruption and coronal mass ejections (CMEs; e.g. Liu et al., 2005; Jiang et al., 2008; Guo et al., 2010; Shen et al., 2012). There are a few studies considering the relationship between large-scale CMEs and small-scale surges/jets. A part of surges/jets associated CMEs have no associations with EPs (Munro et al., 1979). Moreover, there is a close temporal and spatial relationship between a well-observed emerging flux region (EFR), surge and its associated jet-like CMEs without a filament involved in the surge–CME event (Liu et al., 2005b). Besides, Liu (2008) divided surges into three types: jet-like, diffuse, and closed loop. The author found that the jet-like surges were always associated with jet-like CMEs, the diffuse surges were associated with wide-angle CMEs and the closed-loop surges were not associated with CMEs.

Recent studies found a close relationship between the surges occurrence and the formation, evolution and eruption of filaments (see, e.g. Guo et al., 2010, Joshi et al., 2016; Chen et al., 2018). A few studies have shown that there is a close correlation between filament formation and surge activity. For the first time, Zirin (1976) reported a short-lived filament produced by a surge ejection. Liu et al. (2005) also found that some filaments can be rapidly formed in the corona by trapping the cool material supplied by surges. By examining the eruptive event located at the active region (AR) periphery, Li et al. (2015) found that the filament eruption caused a blowout jet and produced an M4.0 flare, which led to a CME. For the loop-shaped filament located in the east side of the surge, Li & Zhang (2013) demonstrated that the interaction between erupting surge and a filament caused “peel off” of the filament and add mass into the flux rope body, which resulted in a failed filament eruption.

Based on the of analysis of recurrent surges with apparent rotational motions and nearby filament, Bong et al. (2014) argued that recurrent reconnections between the twisted filament and a large untwisted flux tube of the surge can trigger the transfer of helicity from the twisted to the untwisted system. Such mechanism could explain the observed evacuation of filament material to the surge, as well as the filament disappearance. A filament eruption caused by recurrent surges/jets, followed by an M2.5 two-ribbon flare and a CME has been reported by Guo et al. (2010). The authors found that the continuous mass with momentum loaded by the surge activities to the filament channel could make the filament unstable and cause it to erupt. Investigating the triggering, activation, and ejection of an eruptive prominence that occurred in a multi-polar flux system of AR NOAA 11548 on 2012 August 18, Joshi et al. (2016) found that during the pre-eruptive phase, the formation of a blowout jet, associated with the eruption of a cool flux rope caused the prominence activation. Afterwards, the prominence erupted, that leads to an M1.8 flare and a partial halo fast CME. The authors argued that the EP is a complex, multi-step phenomenon in which a combination of internal (tether-cutting (TC) reconnection) and external (i.e., pre-eruption coronal activities) processes are involved. Dhara et al. (2017), studying two successive eruptions of two parts of a filament in AR NOAA 11444 on 2012 March 27, found the pre-flare brightening below first filament part that resulted in a jet-like eruption. This eruption via TC mechanism, most probably activated the filament part, which later erupted accompanied by C5.3 class flare. The eruption of the second filament part was triggered by removal of the overlying arcade loops via reconnection process. Both filament eruptions produced high speed (~ 1000 km/s) CMEs. A detailed study of the filament eruption onset (Chen et al., 2018) shows that flux convergence and cancellation, bidirectional jets, as well as the topological changes of hot loops caused filament activation, during which the filament surprisingly splits into three branches. Later, the slow rising high-lying branch abruptly accelerated causing a two-ribbon flare, while the two low-lying branches remained stable, forming a partial eruption. The filament eruption did not cause an obvious CME.

In this case study, we aim to examine the surge eruption that appeared to trigger the EP on 2014 March 14, as is suggested in Dechev et al. (2018). Our main goal is to investigate in detail the EUV precursor eruption signatures in the source region, the surge eruption and EUV brightening, and to clarify the crucial role of the surge eruption in EP initiation. In our previous study (Dechev et al., 2018, hereafter Paper I), which was mainly focused on the prominence activation and eruption, was found that the surge and the associated EP are parts of a complex, multi-step phenomenon, in which two flares, partial-halo CMEs and post-flare loop arcades were involved. Here we present a detailed multi-wavelength study of the surge evolution and kinematics. A special attention was paid to the interaction between the surge and ambient magnetic fields. The surge observations and instrumental data are described in Section 1. In Section 2 we provide the details of our analysis and describe the observational results. The discussion and interpretation of our results and conclusions are presented in Section 3.

1. Observations and Data reduction

1.1. Overview of the surge event

The surge was observed in AIA field of view (FOV) above the southeastern limb on 2014 March 14 between 08:12 and 09:16 UT (Fig. 1). It appeared at the same position angle (PA) where the associated EP was observed, i.e. in the filament channel located in an young short-lived AR - SPoCa: SOL2014-03-14T04:081 still in its emergence phase (see Paper I). The surge source region includes several causally related small-scale eruptive events (Paper I, Table 1). These eruptions appeared ephemeral in AIA FOV but they played a crucial role for the surge and filament activation and eruption. One of them occurred before the surge onset and other two eruptions accompanied its eruption evolution. The EP lasted between 07:33 and 11:48 UT, so the surge took place during early stage of the prominence activation when only the slowly rising of EP massive flux rope (MFR) was observed. The surge and associated filament were surrounded by multiple-arcade helmet streamer, which has a complex magnetic configuration (Fig. 2). Such configuration is favorable for sympathetic events production (e.g. Yang et al., 2012).

The surge firstly appeared on the limb at 08:12 UT as a compact bright closed loop that radially rose up until 08:23 UT. After 08:27 UT, the surge split up vertically into two bundles containing many fine threads: northern, large and tight one and southern, smaller and loose-fitting one. Two bundles rose up along a slightly curved trajectory that outlined the overlying coronal magnetic loops. Because of the same PA of the EP and the surge, the most part of the slow rising EP MFR above the limb was obscured by the bright surge. Moreover, as can be seen in Fig. 1 and Fig. 2, the pictures of surge-EP event are more complicated because of the two low coronal loops from multiple-arcade system, which are cospatial with the surge and EP in the plane of sky. At 08:52 UT the surge reached a maximum height of ~ 73 Mm and then it began to move downward along the same trajectory. Its apparent plasma draining was observed until 09:16 UT, when the surge completely disappeared. It is noteworthy, that the surge was first significant eruption in a chain of physically linked sympathetic events appearing in a single source region (see Paper I).

1.2. Data reduction

For our analysis we used images taken with 24 s cadence in the 304 Å He II, ~ 0.05 MK) passband of AIA/SDO (Lemen et al., 2012). To trace the EP evolution at different heights in the chromosphere and in the corona we used also images in the 335 Å (Fe XVI, ~ 2.8 MK), 211 Å (Fe XIV, ~ 2 MK), 193 Å (Fe XII, Fe XXIV, ~ 1.25 MK), 171 Å (Fe IX, ~ 1 MK), 131 Å (Fe VIII, Fe XXI; ~ 10 MK), and 94 Å (Fe XVIII, ~ 6 MK) AIA channels with 1 minute cadence. We used level 1 reduced data, i.e. with the dark current removed and the flat-field correction applied. All the data were processed with the standard procedures, included in SolarSoftWare.

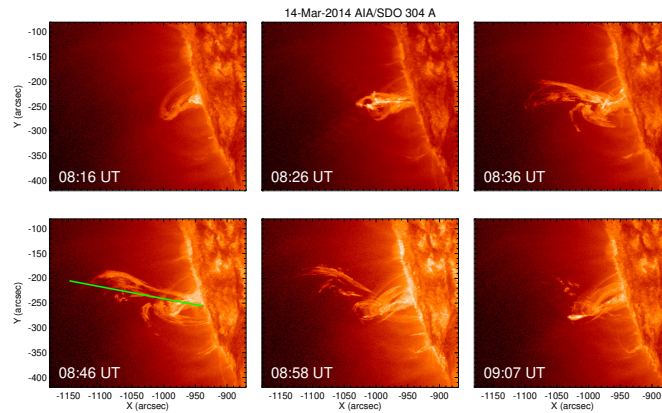


Fig. 1. A sequence of AIA 304 Å images showing the surge activity on 2014 March 14 in AR SPoCa: SOL2014-03-14T04:081. The green line overlaid on the snapshot of 08:46 UT indicates the optimum 5'' narrow slice along the surge propagation, from which the time-distance plot (Fig. 5, left panel) has been generated.

2. Results

2.1. EUV brightening of surge-EP event

By a careful examination of the dynamical activities and EUV brightening at all AIA channels, we divide all of the activity during the surge-EP event into four episodes with a specific brightening evolution (Fig. 3). Figure 4 shows the intensity profiles in the AIA 94, 131, 171, 193, 211, 304, and 335 Å channels. The light-curves are obtained by integrating of the intensity over the area outlined with a green box in the AIA 304 Å image (Fig. 2, top). The green box embraced the lower parts of surge, EP and lower coronal loop, which were overimposed on the sky plane that allow us to search for EUV signatures of possible interactions between them.

2.1.1. First EUV brightening episode. The first episode began before the filament activation (04:48 UT) and lasted up to the surge occurrence at 08:12 UT. The Extreme Ultraviolet Imager (EUVI) 195 Å images of STEREO B confirm the appearance of multiple dynamic activities in the vicinity of a twisted filament before its activation.

Moreover, the presence of large EUV coronal loops connecting the activity site to distant parts of the AR suggests that multiple flux systems existed close to the filament channel (Paper I). After the filament activation (07:33 UT), when the EP MFR already slowly rose, the early pre-flare signatures can

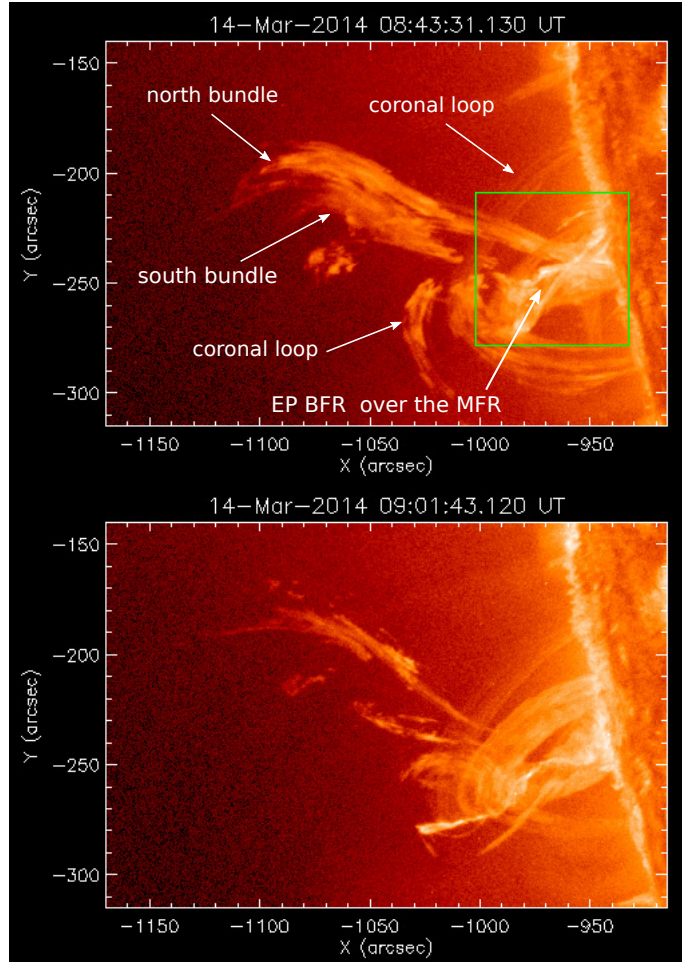


Fig. 2. Top panel: AIA 304 Å image at 08:43 UT (rising phase) showing the complex coronal structure above the source region and underneath the multi-arcade streamer containing a surge, EP MFR and BFR, and coronal loops overimposed on the sky plane; green boxed region was used for intensity analysis. Bottom panel: AIA 304 Å image at 09:01 UT showing the complex coronal structure simplification during the surge downflow phase.

be seen at 08:07 UT in the form of flare-like loop that was observed on the limb in all AIA channels at the position of the surge-EP event. This obvious brightening below the EP MFR gives us a clue that pre-flare reconnection process might be involved in the onset of surge eruption (e.g. Liu et al., 2010; Xu et al., 2017, Chen et al., 2018). In fact, at 08:10 UT, two minutes before the surge onset first eruption was visible at the limb close to the EP MFR footpoints.

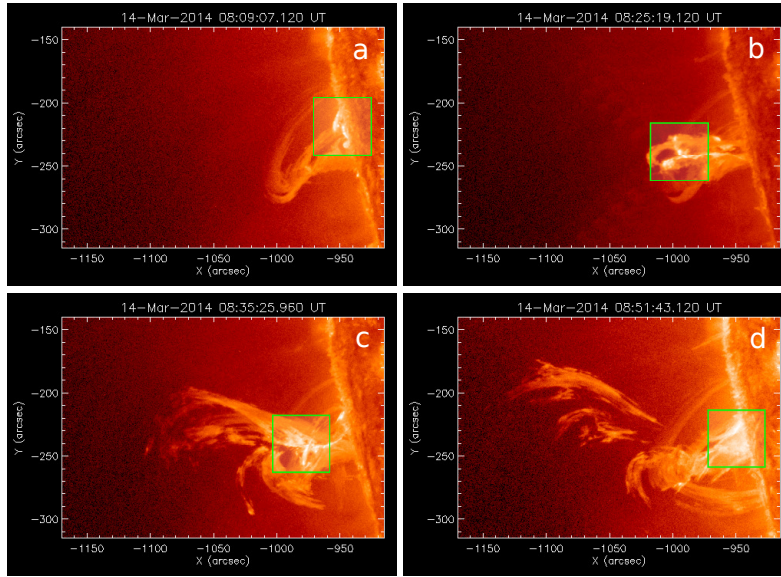


Fig. 3. Four EUV brightening episodes at the time of their maximum brightness. The green boxes localize the projected brightening areas.

2.1.2. Second EUV brightening episode. The second episode covered the early stage of surge eruption (08:12-08:25 UT) when the surge rose as a narrow bright closed loop. Meanwhile, at 08:16 UT second eruption appeared close to the surge and EP MFR footpoints, which possibly have contribution to the surge brightening. At 08:25 UT, when the surge covered the EP MFR and reached lower coronal loop, the first extensive EUV brightening was observed. In addition, an enhanced intensity was observed in the places where parts of the surge, EP MFR and lower coronal loop were co-spatial. As one can see in Fig. 4, after the surge onset the intensity in all EUV channels began to enhance. The 304 \AA light curve displays rapid enhancement with a maximum at 08:26 UT. The light curves of all other high temperature EUV channels display lower local maximums between 08:20 and 08:25 UT.

2.1.3. Third EUV brightening episode. The third brightening episode began just after the maximum of 304 \AA intensity (08:26 UT) and lasted until 08:46 UT. It demonstrated several dramatic events, such as the surge vertical splitting and first observational signatures of the EP BFR origin at 08:27 UT. Besides, the intensity integrated flux in all EUV channels, except 211 \AA underwent small short-time diminishing up to 08:32 UT, when second strong brightening began in the region of overlapped events (Fig. 2). Between 08:32 and 08:43 UT the intensity in high temperature channels showed impulsive behavior with maximum values at around 08:37 UT when the EP BFR was for the first time distinguished. At 08:46 UT the EP BFR was well visible as narrow kinked loop with footpoints closely located to the surge footpoints.

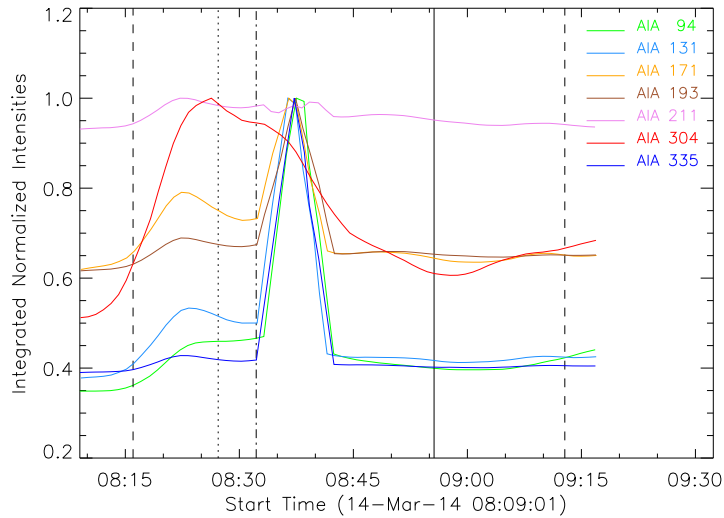


Fig. 4. Normalized integrated intensities in all AIA channels obtained for the area in green box overlotted in Fig. 2 (top panel). Two vertical dashed lines indicate start and end of the surge. The solid black line points out the time of surge maximum height. The dotted line indicates the time of the onset of vertical surge splitting and EP BFR appearance. Dash-dotted line indicates the onset of strong impulsive brightening.

At that time first signatures of simplification of the surge-EP events were observed. The 304 Å light curve displays more gradual behavior and after its maximum the intensity slowly diminished until 08:56 UT when the surge had a maximum height, i.e. just before the surge downflow phase. Two minutes before the surge maximum height, at 08:54 UT third eruption appeared close to the surge and EP footpoints, which most probably have contribution for brightening enhancement at the footpoints.

2.1.4. Fourth EUV brightening episode. The fourth episode covered the surge downflow phase, which was accompanied by BFR development and rising. During this episode, dynamical enhancement of the EUV brightening at the footpoints of surge, BFR and the lower parts of BFR legs was observed. Moreover, at 08:54 UT a third eruption appeared close to the surge and EP footpoints, which might also had contribution to the footpoints brightening enhancement.

2.2. The surge kinematics

To analyze quantitatively the surge upward and downward motions, we chose 5" wide slice located along the surge propagation direction (green line in Fig. 1). We have used the slice to construct a time-slice plot (Fig. 5, left panel) that allows us to measure the surge height during its evolution. In the right

Table 1. Summary of the surge evolution and associated events

Time UT	Observations
08:07	A flare-like loop was observed on the limb in all AIA channels at the position of the surge and EP.
08:09	Onset of 1st EUV brightening episode.
08:10	First eruption appearance close to the EP MFR footpoints.
08:12	A surge started and rose as a bright closed loop. Onset of 2nd EUV brightening episode.
08:16	Second eruption appearance close to the surge and EP MFR footpoints.
08:23	A surge fully covered the EP MFR and reached south leg of lower coronal loop; In the region of covering first brightening was observed.
08:25	In surge covered upper parts of EP MFR and coronal loop first extensive EUV brightening was observed.
08:27	The surge split of two bundles: large north and narrow south ones; the large middle part of overimposed events was brightened; First signature of EP BFR origin was observed.
08:32	Second strong brightening began in the region of overimposed events
08:35	Onset of 3rd EUV brightening episode.
08:37	The brightening in this region observed in high temperature channels reached maximum intensity. First identification of EP BFR.
08:46	The surge reached a maximum height of 73 Mm. The surge plasma began to move back to the chromosphere. Onset of 4th EUV brightening episode. The surge complex picture began to simplify. The EP BFR was well visible as narrow kink-shaped loop with footpoints close to surge footpoints.
08:54	Third eruption appearance close to the surge and EP footpoints; The surge two bundles were well separated from each other.
08:58	After that time, the surge plasma downflow was accompanied brightening enhancement at the footpoints of surge and EP MFR and BFR.
09:13	Last stage of surge downflow after that time was obscured by the bright EP MFR and BFR.

panel of Fig. 5 the time profile of the surge projected height is presented. The surge rising phase was between 08:12 and 08:56 UT. The rising phase showed two subphases: acceleration - between 08:12 and 08:32 UT and deceleration - between 08:32 and 08:56 UT (Fig. 5, right panel). The surge downflow phase was traced from 08:46 UT until 09:13 UT at a height of 22 Mm. The last part of the surge downflow between 22 Mm height and chromosphere was obscured by the bright system of EP MFR and BFR.

To quantitatively estimate the surge acceleration subphase, third-order polynomial fit was applied. The speed of the rising surge increased from 3 km/s to 65 km/s and acceleration changes in the range 0.5-120 m/s². The standard error of the regression estimation is 21.6 ± 0.63 Mm, where the value of 21.64 Mm is the mean height predicted by the applied model. The estimation of the surge deceleration subphase was made by second-order polynomial fit. During this subphase, the surge rose with decreasing speed from 60 km/s to 13 km/s at constant negative accelerations of -54.8 m/s². The standard error of the

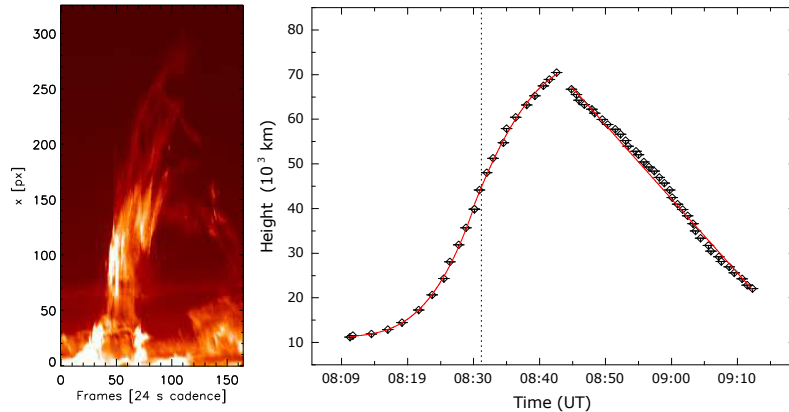


Fig. 5. Left: Time-distance plot made by 5'' narrow slice from AIA 304 Å images (green line in Fig. 1). Right: Height-time profile of the surge determined by the time-distance plot. The vertical dotted line divides the acceleration and deceleration surge phases.

regression estimation is 58.8 ± 1 Mm, where 58.8 Mm is the predicted mean height.

During the surge downflow phase, the surge body underwent dynamical simplification, which was accompanied by the gradually fading and disappearing of many threads in its body. That does not allow precise tracing of a single thread. The surge simplification was partially due to the untwisting motion and decreasing number of the threads visible in EUV lines, as well. By this reason, we estimated the downflow phase with linear fit and found that the speed of plasma downflow was 27 km/s.

3. Summary and Discussions

3.1. Summary

The surge appeared in the AR filament channel underneath multipolar arcade helmet streamer, i.e. below the so-called pseudo-streamers (e.g. Hundhausen, 1972; Wang et al., 2007), where a multi-polar flux system was formed (Titov et al., 2012; Joshi et al., 2016). In recent study of field connectivity for the eruptions on 2010 August 1–2, Schrijver & Title (2011) found evidence that all involved source regions were connected by structural features such as separatrix surfaces, separators, and quasi-separatrix layers. By a comprehensive structural analysis of pseudo-streamers Titov et al. (2012) showed that they contains several separators, all of which are connected to a basic null point. They found that an external perturbation in the null point neighborhood should trigger there an external interchange reconnection, while an internal perturbation hear to the separatrix surface bald patches should trigger an internal tether-cutting reconnection. The authors also showed that the magnetic environment in which such eruptions occur allows one to get deeper understanding of the relationship between linked eruptions. Moreover, the authors,

using recent MHD model of sympathetic eruptions (Török et al., 2011), argued that magnetic reconnection at these types of separators is likely a key process in sympathetic eruptions, because it controls how magnetic fluxes are redistributed between the lobes of pseudo-streamers during eruptions. Therefore, our multi-arcade streamer had a favorable magnetic configuration for producing sympathetic eruptions. In fact, the surge was first apparent eruption in a chain of physically linked sympathetic events appearing in a single source region (see Paper I). Summary of activity associated with various phases of the surge-EP event is given in Table 1. The main results of the study and their discussions are listed below.

3.2. Discussions

The surge motion clearly shows two main phases: upward and downward. The upward phase was consisted of two subphases: accelerative and decelerative ones. During the accelerative subphase, the surge rose with growing speed in the range 3-65 km/s and an increasing acceleration between 0.5 m/s^2 and 129 m/s^2 . During the decelerative subphase, the surge rose with a constant deceleration of -54.8 m/s^2 and speeds from 60 km/s to 13 km/s. During the downflow phase, the surge plasma flowed back to the chromosphere with a constant speed of 27 km/s. It is interesting that the nearest event similar to the studied surge was the confined partial filament eruption on 2014 December 24 (Cheng et al., 2018), during which the filament FR undergoes vertical splitting due to internal reconnection. The two events show very similar height-time profiles and spatial scales of their rising. However, there is an essential difference between their rising velocity and acceleration. In the case of filament rising they are an order of magnitude larger than those of the surge.

The surge-EP event on 2014 March 14 showed four EUV brightening episodes, which reveal different kinds of brightenings, resulting from different heating mechanisms.

During the first episode (04:48 – 08:12 UT), two significant events appeared: a small flare-like loop at the limb with apparent EUV brightening and an eruption close to the EP MFR footpoints. The bright flare-like loop can be interpreted as a radiative signature of the small-scale TC reconnection beneath the MFR, which is due to the flux cancellation between the opposite polarity magnetic fields below the EP MFR (Moore & Roumeliotis, 1992; Sterling & Moore, 2005). Such brightenings at or near the polarity inversion line (PIL), coincident with emerging and/or canceling magnetic flux are considered as precursors of the flare and filament eruption (Chifor et al., 2007; Kim et al., 2007; Liu et al. 2009; Sterling, Moore, & Freeland, 2011). On the other hand, the first eruption appearance close to the MFR footpoints, also suggests a small-scale pre-flare TC reconnection taking place in the filament channel (e.g. Moore & Roumeliotis, 1992; Moore et al., 2001). Moreover, the formation of a close underlying flare loop, observed in the EUV images during the surge, suggests the magnetic reconnection as a driver of surge and associated filament eruption (e.g. Dhara et al., 2017). Besides, Sterling et al., (2015, 2016) clearly found a casual relationship between minifilament eruptions and jet activity. They suggest that the eruptive activities at relatively smaller-scales

may not only cause surges/jets, but can further lead to the destabilization of a large-scale filament FR.

During the second episode (08:12 – 08:25 UT), the surge appeared and evolved as a bright closed-loop, i.e. it belongs to the closed-loop type surges according to the classification of Liu (2008), which are not associated with CMEs. The surge rise was accompanied by the EUV brightening enhancement, especially in AIA 304 Å channel. The 304 Å flux reached a maximum value in the end of this episode, at the time when surge upper part, EP MFR and lower coronal loops were observed as overimposed events in the sky plane. The brightness distribution co-spatial with overimposed event's parts, suggests that the surge-EP system and two coronal loops were closely located each other, which infers the interactions between the surge and other events. In addition, the EUV multiwavelength brightening is one of the observational signatures of TC reconnection (e.g. Yurchyshyn et al., 2006) that is often observed during the interaction of nearby FRs (Chen et al. 2016, and references therein). Hence, the brightening could be considered to be produced by a reconnection between the erupting surge and its surrounding structures (see, e.g. Attrill et al., 2007, 2009; Mandrini et al., 2007), resulting from the intercoupling and interaction of multiple flux loop systems of the surge-EP event (e.g. Zhang et al., 2007; Yang et al., 2011).

The strong impulsive brightening during the third episode (08:32 – 08:43 UT) suggests that the reconnection and magnetic flux transfer took place in the collision regions of the surge-MFR-loops configuration, where the plasma was heated to a few MK (e.g. Jiang et al., 2013; Li & Ding, 2017, and references therein). During the surge merging via TC reconnection with the surrounded magnetic structures, it underwent bifurcation and horizontal splitting of two vertical bundles that is intrinsic for the separation of collided FRs (e.g. Kumar et al., 2010; Chandra et al., 2011; Chen et al., 2016). The surge horizontal splitting was conditioned by the asymmetric behavior of surge eruption that is similar to such splitting of the filament eruptions (Tripathi et al. 2006a) and minifilaments (Panesar et al. 2017). In addition, a horizontal splitting may occur if the tension force of the overlying flux varies sufficiently along a filament channel such as multi-flux pseudo-streamer above the surge event (see Cheng et al., 2018 and references therein). Moreover, the reconnection may cause changes in the plasma distribution and in the connectivity of surge field line footpoints. In addition, two types of TC reconnection probably took place in the surge interactions: an internal reconnection between the surge and EP MFR because they share a common filament channel and external reconnection between the surge and ambient lower coronal loop (Su et al., 2007). It is noteworthy that the surge splitting was a crucial process for its further evolution because, afterward, it manifested a behavior typical for diffuse type surges or blowout type following the nomenclature of Moore et al. (2010, 2013), which are usually associated with very wide CMEs (halo or partial-halo) (Liu, 2008). After the bifurcation, the eruptive behavior of two bundles suggests "sling-shot" effect due to TC reconnection, which produces a whip-like plasma motion (e.g. Jiang et al., 2013). In addition, the more steady eruptive behavior of the northern surge bundle with respect to the southern one suggests that the surge eruption is consistent with one of the simulation scenarios proposed by Kliem et al. (2014), that considers an eruption of two nearby FRs, vertically arranged

above the photosphere. Another essential feature of the third episode was the first appearance of EP BFR and its formation beneath the EP MFR that were co-temporarily observed with the surge splitting. Besides, in the beginning of 3rd episode, the patch-like brightening appeared in the filament channel near to the footpoints of northern surge bundle. The patch brightening and followed jet-like bright flow could be signatures of the reconnection that occurred in the lower layers and a signature of TC mechanism, which could have activated the second filament FR that later erupted as BFR (see, e.g. Dhara et al., 2017; Chen et al., 2018), although other mechanisms should not be excluded.

During the fourth episode (08:46 – 09:16 UT), only the enhanced brightening at the footpoints of surge-EP system and the thin BFR were observed in high temperature lines. During the surge downflow, the plasma flowed back along the lifting coronal field and impact the chromosphere at the surge-EP footpoints that generate significant brightening through kinetic energy dissipation (e.g. Gilbert et al., 2013; Innes et al., 2016). We do not exclude some other mechanisms, such as impact ionization (Downs et al., 2013; Petralia et al., 2016) or reconnection between the field channeling impact plasma and the low-lying loops (Gilbert et al., 2013), which might play some role in this brightening. Moreover, third eruption that appeared at 08:54 UT close to the footpoints of surge-EP system, might have contribution to the footpoints brightening. During this episode, the BFR rose up with a speed larger than those of the upper MFR accompanied by writhing of its loop. In addition, it rose up with a speed larger than those of the upper MFR. At 09:16 UT, when the surge is not already visible in the AIA FOV, the BFR reached MFR and merged with them (see Paper I). It should be noted that the BFR kept high brightness during whole its evolution, which could be explained with the continual surge mass impact/transfer at the BFR footpoints up to the surge disappearing. As Gilbert et al. (2013) noted, although the compression mechanism is dominant over the reconnection, both are possibly occurring since the falling plasma undoubtedly carries frozen-in magnetic flux.

3.3. Conclusions

In conclusion, in this study we report a rare case of a non-standard surge that showed unusual eruptive behavior conditioned by a significant topological change, as well a horizontal splitting during its eruption. Moreover, we found multi-step surge EUV brightenings produced by interaction between the surge, EP and ambient coronal loops, which caused the surge bifurcation. These findings observationally support one of the unstable configurations scenarios of Kliem et al. (2014), which simulates the eruption of two nearby vertical FRs. We also found that the surge played a key role in triggering the BFR, whose dominant instability was crucial for the further behavior of the EP. Finally, further investigations involving similar magnetic structure with high temporal and spatial resolution observations would be helpful to fully understand the physical mechanisms of solar eruptions and their causal linkage, as well.

Acknowledgements

We thank the anonymous referee for her/his constructive suggestions and comments, which helped to improve this manuscript. We thank the SDO teams

for providing their excellent observations for the present study. This research is co-funded by the Bulgarian National Science Fund under Grants DH 08-1/13.12.2016, DN 18-13/12.12.2017 and KP-06-India/14 (19-Dec-2019).

References

- Attrill, G. D. R., Engell, A. J., Wills-Davey, M. J., et al., 2009, *ApJ*, 704, 1296
Attrill, G. D. R., Harra, L. K., van Driel-Gesztelyi, L., & Démoulin, P., 2007, *ApJ*, 656, L101
Beck, C., Bellot Rubio, L. R., Schlichenmaier, R., & Sütterlin, P., 2007, *A&A*, 472, 607
Bong, Su-Chan; Cho, Kyung-Suk; Yurchyshyn, Vasyl, 2014, *JKAS*, 47, 311.
Bruzek, A., & Durrant, C. J., 1977, *Illustrated Glossary for Solar and Solar-Terrestrial Physics*, Astrophysics and Space Science Library (Dordrecht: Reidel)
Canfield, R. C., Reardon, K. P., Leka, et al., 1996, *ApJ*, 464, 1016
Chae, J., Qiu, J., Wang, H., & Goode, P. R., 1999, *ApJL*, 513, L75
Chandra, R., Jain, R., Uddin, W., et al., 2006, *Solar Phys.*, 239, 239
Chandra, R., Schmieder, B., Mandrini, C. H., et al., 2011, *Solar Phys.*, 269, 83
Chen, H., Duan, Y., Yang, J., Yang, Bo, Dai, J., 2018, *ApJ*, 869, 78.
Chen, H., Zhang, J., Li, L., & Ma, S., 2016, *ApJ*, 818, L27
Cheng, X., Kliem, B., & Ding, M. D., 2018, *ApJ*, 856, 48
Chifor, C., Tripathi, D., Mason, H. E., Dennis, B. R., 2007, *A&A*, 472, 967
Dechev, M.; Duchlev, P.; Koleva, K., 2018, *BlgAJ* 28, 60. (Paper I)
Dhara, S. K., Belur, R., Kumar, P., et al., 2017, *Solar Phys.*, 292, 145.
Downs, C., Linker, J. A., Mikic, Z., et al., 2013, *Science*, 340, 1196
Engell, A. J., Siarkowski, M., Gryciuk, M., et al., 2011, *ApJ*, 726, 12
Gaizauskas, V., 1996, *Solar Phys.*, 169, 357
Gilbert, H. R., Inglis, A. R., Mays, M. L., et al., 2013, *ApJL*, 776, L12
Guo, J., Liu, Y., Zhang, H., et al., 2010, *ApJ*, 711, 1057
Guo, Juan, Liu, Yu, Zhang, Hongqi, et al., 2010, *ApJ*, 711, 1057.
Hundhausen, A. J. (ed.), 1972, *Coronal Expansion and Solar Wind* (Berlin: Springer)
Innes, D. E., Heinrich, P., Inhester, B., & Guo, L.-J., 2016, *A&A*, 592 A17
Jiang, Y., Hong, J., Yang, J., et al., 2013, *ApJ*, 764, 68
Jiang, Y., Shen, Y., Yi, B., Yang, J., & Wang, J., 2008, *ApJ*, 677, 699
Joshi, B., Kushwaha, U., Veronig, A. M., Cho, K.-S., 2016, *ApJ*, 832, 130.
Kim, S., Moon, Y.-J., Kim, K.-H., et al., 2007, *PASJ*, 59, 831
Kliem, B., Török, T., Titov, V. S., et al., 2014, *ApJ*, 792, 107
Kumar, P., Manoharan, P. K., & Uddin, W., 2010, *ApJ*, 710, 1195
Kurokawa, H., & Kawai, G., 1993, in *ASP CS 46, IAU Colloq. 141: The Magnetic and Velocity Fields of Solar Active Regions*, ed. H. Zirin, G. Ai, & H. Wang (San Francisco, CA: ASP), 507
Lemen, J. R., Title, A. M., Akin, D. J., et al., 2012, *Solar Phys.*, 275, 17
Li, Y. & Ding, M. D., 2017, *ApJ*, 838, 15
Li, K. J., Li, J., Gu, X. M., & Zhong, S. H., 1996, *Solar Phys.*, 168, 91
Li, Ting & Zhang, Jun, 2013, *ApJ*, 770, L25.
Li, Xiaohong; Yang, Shuhong; Chen, Huadong; Li, Ting; Zhang, Jun, 2015, *ApJ*, 814, L13.
Liu, C., Deng, N., Liu, R., Ugarte-Urra, I., Wang, S., & Wang, H., 2011, *ApJ*, 735, L18
Liu, R., Liu, C., Wang, S., Deng, N., & Wang, H. 2010, *ApJL*, 725, L84
Liu, W., Wang, T.-J., Dennis, B.R., Holman, G.D., 2009, *ApJ*, 698, 632
Liu, Y., 2008, *Solar Phys.*, 249, 75
Liu, Y., & Kurokawa, H., 2004, *ApJ*, 610, 1136
Liu, Y., & Zhang, H., 2001, *A&A*, 372, 1019
Liu, Y., Kurokawa, H., & Shibata, K. 2005a, *ApJ*, 631, L93
Liu, Y., Su, J. T., Morimoto, T., Kurokawa, H., & Shibata, K., 2005b, *ApJ*, 628, 1056
Madjarska, M. S., Doyle, J. G., & de Pontieu, B., 2009, *ApJ*, 701, 253
Mandrini, C. H., Nakwacki, M. S., Attrill, G. D. R., et al., 2007, *Solar Phys.*, 244, 25
Moore, R. L., & Roumeliotis, G., 1992, in *IAU Coll. 133, Eruptive Solar Flares*, ed. Z. Svestka, B. V. Jackson, & M. E. Machado (Berlin: Springer), 69
Moore, R.L., Sterling, A.C., Hudson, H.S., Lemen, J.R., 2001, *ApJ*, 552, 833
Moore, R. L., Cirtain, J. W., Sterling, A. C., & Falconer, D. A. 2010, *ApJ*, 720, 757
Moore, R. L., Sterling, A. C., Falconer, D. A., & Robe, D. 2013, *ApJ*, 769, 134
Munro, R. H., Gosling, J. T., Hildner, E., et al., 1979, *Solar Phys.*, 61, 201
Panesar, N. K., Sterling, A. C., & Moore, R. L., 2016, *ApJL*, 822, L23

- Panesar, N. K., Sterling, A. C., & Moore, R. L., 2017, *ApJ*, 844, 131
 Pariat, E., Antiochos, S. K., & DeVore, C. R., 2010, *ApJ*, 714, 1762
 Petralia, A., Reale, F., Orlando, S., & Testa, P., 2016, *ApJ*, 832, 2
 Reidel), 69. Rust, D. M., 1968, in *IAU Symp. 35, Structure and Development of Solar Active Regions*, ed. K. Otto (Cambridge: Cambridge Univ. Press), 77
 Schmieder, B., Golub, L., & Antiochos, S. K., 1994, *ApJ*, 425, 326
 Schmieder, B., Mein, P., Simnett, G. M., & Tandberg-Hanssen, E., 1988, *A&A*, 201, 327
 Schmieder, B., Shibata, K., van Driel-Gesztelyi, L., & Freeland, S. 1995, *Solar Phys.*, 156, 245
 Schmieder, B., van Driel-Gesztelyi, L., Gerlei, O., & Simnett, G. M., 1993, *Solar Phys.*, 146, 163
 Schrijver, C. J. & Title, A. M., 2011, *J. Geophys. Res.*, 116, A04108
 Shen, Y., Liu, Y., Su, J., & Deng, Y., 2012, *ApJ*, 745, 164
 Shibata, K., Ishido, Y., Acton, L. A., et al., 1992, *PASJ*, 44, L173
 Shibata, K., Nishikawa, T., Kitai, R., & Suematsu, Y., 1982, *Solar Phys.*, 77, 121
 Shimojo, M., Shibata, K., & Harvey, K. L., 1998, *Solar Phys.*, 178, 379
 Sterling, A. C., 2000, *Solar Phys.*, 196, 79
 Sterling, A.C., Moore, R.L., 2005, *ApJ*. 630, 1148.
 Sterling, A. C., Moore, R. L., Falconer, D. A., & Adams, M., 2015, *Nature*, 523, 437
 Sterling, A. C., Moore, R. L., Falconer, D. A., et al., 2016, *ApJ*, 821, 100
 Sterling, A. C., Shibata, K., & Mariska, J. T., 1993, *ApJ*, 407, 778
 Su, J., Liu, Y., Kurokawa, H., et al., 2007, *Solar Phys.*, 242, 53
 Titov, V. S., Mikic, Z., Török, T., Linker, J. A., & Panasenco, O., 2012, *ApJ*, 759, 70
 Török, T., Panasenco, O., Titov, V. S., et al., 2011, *ApJ*, 739, L63
 Tripathi, D., Isobe, H., & Mason, H. E., 2006, *A&A*, 453, 1111
 Uddin, W., Jain, R., Yoshimura, K., et al., 2004, *Solar Phys.*, 225, 325.
 Uddin, W., Kumar, P., Srivastava, A. K., & Chandra, R., 2010, in *Magnetic Coupling between the Interior and Atmosphere of the Sun*, ed. S. S. Hasan & R. J. Rutten (Berlin: Springer), 478
 Uddin, W., Schmieder, B., Chandra, R., et al., 2012, *ApJ*, 752, 70.
 Wang, Y.-M., Sheeley, N. R., Jr., & Rich, N. B., 2007, *ApJ*, 658, 1340
 Xu, Z., Lagg, A., Solanki, S., & Liu, Y., 2012, *ApJ*, 749, 138
 Yang, J., Jiang, Y., Zheng, R., et al., 2011, *Solar Phys.*, 270, 551
 Yang, J., Jiang, Y., Zheng, R., et al., 2012, *ApJ* 745, 9
 Yurchyshyn, V., Karlický, M., Hu, Q., & Wang, H., 2006, *Solar Phys.*, 235, 147
 Zhang, Y., Wang, J., Attrill, G. D. R., et al., 2007, *Solar Phys.*, 241, 329
 Zirin, H., 1976, *Solar Phys.*, 50, 399.